# Greenhouse gases modulate the strength of millennial-scale subtropical rainfall, consistent with future predictions

Fei Guo[1,2,*], Steven C. Clemens[2,*], Yuming Liu[1,3], Ting Wang[1,3], Huimin Fan[1], Xingxing Liu[1], Youbin Sun[1,4,5]

[1]State Key Laboratory of Loess and Quaternary Geology, Institute of Earth Environment, Chinese Academy of Sciences, Xian 710061, China.

[2]Department of Earth, Environmental, and Planetary Sciences, Brown University, Providence, RI 02912-1846, USA

[3]University of Chinese Academy of Sciences, Beijing 100049, China

[4]CAS Center for Excellence in Quaternary Science and Global Change, Xian 710061, China.

[5]Open Studio for Oceanic-Continental Climate and Environment Changes, Pilot National Laboratory for Marine Science and Technology (Qingdao), Qingdao 266200, China.

Corresponding author: Fei Guo (guofei@ieecas.cn) and Steven C. Clemens (steven_clemens@brown.edu)

## Key Points

The new precipitation-sensitive proxy (Ca/Ti) shows persistent millennial-scale East Asian summer monsoon changes over past 650 ka;

Greenhouse gases (GHG) and summer insolation modulate millennial fluctuations of loess Ca/Ti at the precession band but not that of $\delta^{18}$Osp;

Increasing GHG and strong insolation lead to more frequently occurrence of extreme rainfall, consistent with model results.

**Abstract:** Millennial scale East Asian monsoon variability is closely associated with natural hazards through long-term variability in flood and drought cycles. Here we present a new East Asian summer monsoon (EASM) rainfall reconstruction from the northwest Chinese loess plateau spanning the past 650,000 years. The magnitude of millennial monsoon variability (MMV) in EASM rainfall is strongly linked to ice volume and greenhouse gas (GHG) at the 100,000-year earth-orbital eccentricity band and to GHG and summer insolation at the 23,000-year precession band. At the precession band, times of stronger insolation and increased atmospheric GHG lead to increases in the MMV of EASM rainfall. These findings indicate increased extreme precipitation events under future warming scenarios, consistent with model results.

## Plain Language Summary

We present a new East Asian summer monsoon rainfall reconstruction from the northwest Chinese loess plateau over the last 650,000 years. This new precipitation proxy (Ca/Ti) and speleothem $\delta^{18}O$ ($\delta^{18}Osp$) are assessed to illustrate the modulating drivers of magnitude of millennial monsoon variability (MMV) in long-term trend. Wavelet analysis highlights the remarkable ice volume and GHG modulation at 100 kyr band as well as GHG and local insolation forcing at precession band for the MMV of Ca/Ti, but not that of MMV in $\delta^{18}Osp$. The MMV of loess Ca/Ti and $\delta^{18}Osp$ are modulated differently at orbital time scales, implying that these two proxies document different climatic response of millennial-scale monsoon circulations. At the precession band, increasing atmospheric GHG following with larger insolation results in further enhancement in MMV of EASM rainfall, which agrees with the model result and prediction in more frequently occurrence of extreme rainfall under future global warming conditions.

## 1. Introduction

The Chinese loess is a unique terrestrial archive that can well documents East Asian monsoon (EAM) variability at tectonic to millennial timescales (Porter and An, 1995; Liu and Ding, 1998; An, 2000; An et al., 2011). High-resolution loess have revealed persistent millennial-scale (1-10 kyr periodicity) EAM fluctuations spanning the last several glacial cycles (Guo et al., 1996; Ding et al., 1999; Sun et al., 2012, 2016, 2021a; Yang et al., 2014; Wang et al., 2020; Guo et al., 2021), which are dynamically linked with high-latitude abrupt changes in the north Atlantic including Heinrich (H) (Heinrich, 1988; Bond et al., 1992) and Dansgaard-Oeschger (DO) events (Dansgaard et al., 1982, 1993; Bond et al., 1993). This millennial-scale monsoon variability is

superimposed on glacial-interglacial variations (Ding et al., 1999; Sun et al, 2016; Yang et al., 2014; Clemens et al., 2018). Abrupt summer monsoon changes are closely linked to natural hazards such as flood and drought events (Huang et al., 2007; Wu et al., 2017), since summer monsoon plays a leading role in transporting water vapor from low to middle/high latitudes of the northern hemispheres (Webster et al., 1998; Wang and Ding, 2008; Wang, 2009; Guo et al., 2012; Liu et al., 2013; An et al., 2015). Abrupt rainfall events associated with short-term summer monsoon variations have seriously influence on agriculture, food production, water supply and social economic development (Ding and Chan, 2005; Huang et al., 2007; Yancheva et al. 2007; Cook et al. 2010; Li et al., 2017; Wu et al., 2021). However, how these flood/drought events are affected by both natural and anthropogenic factors remains poorly constrained. Understanding the mechanisms that modulate the magnitude of millennial-scale variability (MMV) is of critical importance for the scientific community as well as policy makers.

A number of well-dated, high-resolution speleothem $\delta^{18}O$ records have been developed in recent years (Wang et al., 2001, 2008; Cheng et al., 2016), providing the opportunity to examine the underlying relationship(s) between East Asian monsoon MMV and potential longer-term (orbital-scale) modulators. Cheng et al., (2016) hypothesized, on the basis of an East Asian composite speleothem $\delta^{18}O$ record ($\delta^{18}Osp$), that periods of maximum Northern Hemisphere summer insolation correspond to weaker millennial-scale variability. Subsequently, however, Thirumalai et al. (2020) showed that precession does not modulate the MMV of $\delta^{18}Osp$ and postulated that it is, instead, modulated by internal processes related to the cryosphere. This work also raised the possibility that $\delta^{18}Osp$ is decoupled from regional Asian monsoon rainfall over millennial timescales (Zhang et al., 2018). As such, two important outstanding questions remain; is there a reliable proxy for East Asian summer monsoon (EASM) rainfall at the millennial timescale and what modulate the MMV thereof?

To address these questions, we have generated a high-resolution summer monsoon proxy (Ca/Ti) from Linxia (LX, 103.63°E, 35.15°N, 2200 m a.s.l.) on the western Chinese loess plateau (CLP) (Fig. S1). The Ca/Ti ratio is a precipitation-sensitive proxy linked to summer monsoon rainfall (Guo et al., 2021). Low values of Ca/Ti indicate stronger Ca leaching associated with intensified summer rainfall. The new precipitation proxy (Ca/Ti) and $\delta^{18}Osp$ are evaluated to elucidate the modulating drivers of these two proxy records. As discussed in the Results section,

we find that the MMV of Ca/Ti is mainly modulated by ice volume and greenhouse gases (GHG) at the eccentricity band. GHG and summer insolation modulate the MMV of Ca/Ti at the precession band but not that of $\delta^{18}$Osp; $\delta^{18}$Osp MMV is modulated by winter insolation at the eccentricity and obliquity bands. The interpretations of these results are presented in the Discussion section.

## 2. Materials and Methods

Here we present a high-resolution loess record (LX loess profile, 103.63°E, 35.15°N, 2,200 m a.s.l.) from the western edge of the CLP (Fig. S1). At present, mean annual temperature and precipitation in this region are about 8.1°C and 484 mm, respectively, with ~80% of the annual precipitation falling during the summer season (May to September). 203.8 m-long core A (LXA, consisting of 185 m of eolian loess-paleosol sequences, underlain by 17 m of fluvial loess and 1.8 m of sandy gravel layers), 72 m-long core B (LXB) and a 7 m pit were excavated in 2017. Powder samples were collected at 2 cm intervals for analyzing mean grain size (MGS). Meanwhile, each core was scanned at 2-cm resolution by XRF core scanning to obtain elemental intensities.

The upper 18 m is mapped to the OSL dated Yuanbao loess outcrop (~4 kilometers away) (Lai et al., 2006, 2007). The whole 180 m loess chronology has been generated using an independent loess chronology by synchronizing Chinese loess and speleothem $\delta^{18}$O records back to 650 ka (Sun et al., 2021). The first set of control points delineate the loess/paleosol boundaries $S_6$ to $S_0$ matching well with the timing of the glacial terminations/inceptions of speleothem $\delta^{18}$O (Cheng et al., 2009; 2016). The second and third sets of age control points delineate the timing of precessional transition boundaries and abrupt cooling events (Fig. 1), respectively, based on the assumption that the East Asian summer and winter monsoon co-vary with each other at orbital timescales, and millennial-scale abrupt events are synchronous in the northern hemisphere (Hemming et al., 2004; Sun et al., 2012; Rao et al., 2013; Barker et al., 2011; Clemens et al., 2018). The tie points are shown in Fig.1.

Due to weak pedogenesis and high sedimentation rates, millennial-scale oscillations are well preserved in the western and northwestern CLP over the past glacial cycles (Sun et al., 2012, 2016; Guo et al., 2021). Meanwhile, the LX profile is well-suited for reconstructing rapid monsoon changes because it is located in monsoon frontal zone and sensitive to high- and low-latitude climate variability. The MGS reflects grain-size sorting, an indicator sensitive to winter monsoon

variations (An et al., 1990; Porter and An, 1995; Sun et al., 2006). The Ca/Ti ratio reflects precipitation-induced leaching intensity linked to summer monsoon rainfall (Guo et al., 2021). The high resolution $\delta^{18}O$ of Sanbao-Hulu speleothem is an indicator of East Asian monsoon changes at orbital to centennial timescales (Cheng et al., 2009, 2016). Beyond clear glacial-interglacial and precessional fluctuations, high pass filtering (10 ka) of Ca/Ti and MGS in the LX sections shows persistent millennial-scale variations similar to that of Chinese speleothem $\delta^{18}O$ (Fig. 2 and S2).

In order to estimate the MMV, all the raw datasets are linear interpolated at 0.1 kyr interval. The original time series are filtered using a Butterworth filter at a cutoff threshold of 10 kyr (XX-hi-10ka). The standard deviation of millennial-scale variability is applied to reflecting the orbitally evoked modulation and its association with internal and external forcing with 2 ka sliding window (calculation method following the paper from Thirumalai et al., 2020). The spectral result of all the proxies in this paper were conducted by using the Lomb-Scargle periodogram online (https://exoplanetarchive.ipac.caltech.edu/cgi-bin/Pgram/nph-pgram), which could analyze discontinuous time series and remove spurious spectral characteristics (VanderPlas, 2018). Normalized orbital parameters eccentricity, tilt, and precession (ETP), GHG, insolation and benthic $\delta^{18}O$ of LR04 over the past 650 kyr are applied in the wavelet coherence (WTC) calculations to extract maximal phase and amplitude correlations with astronomical, ice volume and greenhouse gases forcing. WTC between time series was performed in a Monte Carlo framework (n = 1, 000) using open source metlab codes (Grinsted et al., 2004).

In this paper, the parameter $\Delta RF_{GHG}$ is regarded as GHG radiative forcing factors and applied in WTC to evaluate the relationship between MMV of Ca/Ti and $\delta^{18}O$ sp. The ΔRFGHG is reconstructed by referencing the content of EPICA ice core greenhouse gases to the modern value. ΔRFGHG is defined as the difference between a certain past GHG level ($[CO_2]$ and $[CH_4]$) and the pre-industrial greenhouse gas level ($[CO_2]_0 = 280$ ppm, $[CH_4]_0 = 700$ ppb) (Ramaswamy et al., 2001). Although $CH_4$ contributes only <5%, we calculated the ΔRFGHG using both $CO_2$ and $CH_4$. The equation used to determine ΔRFGHG is as follows (Li et al., 2017):

$$\Delta RFGHG = \Delta RFCO_2 + \Delta RFCH_4$$

$$= 4.841\ln([CO_2]/[CO_2]_0) + 0.0906(\sqrt{[CO_2]} - \sqrt{[CO2]})_0 + 0.036\ln(\sqrt{[CH_4]}) - (\sqrt{[CH_4]_0}).$$

## 3. Results

The Ca/Ti ratio exhibits distinct glacial-interglacial and precessional variations over the last 650 ka as seen in LR04 $\delta^{18}O$ (Lisiecki and Raymo, 2005) and speleothem $\delta^{18}O$ (Cheng et al., 2009, 2016), respectively (Fig. 1). Both Ca/Ti and $\delta^{18}Osp$ show clear millennial-scale fluctuations overlaying orbital-scale variations. The high frequency millennial signals (isolated with a 10 kyr high pass filter) persist over the last 650 ka for the loess Ca/Ti and speleothem $\delta^{18}O$ records, but the amplitude varies proxy to proxy (Fig. 1a and S2a). Spectral analysis of the raw records and MMV for loess and speleothem records display variable associations with eccentricity- (~100 kyr), obliquity- (~41 kyr), and precession-scale (~23 and ~19 kyr) over the past 650 ka. Loess Ca/Ti variance is mainly concentrated in obliquity with lesser variance in the eccentricity and precession bands (Fig. 2b), indicating prominent ice volume (eccentricity and obliquity) and isolation (precession) forcing. The speleothem $\delta^{18}O$ shows predominant precession-scale variance (Fig. S2a) suggesting strong links to insolation forcing (Cheng et al., 2009, 2016). These results indicate ice volume and insolation play dominated roles in driving changes in loess Ca/Ti and speleothem $\delta^{18}O$, respectively. (Cheng et al., 2009, 2016; Clemens et al., 2010; An et al., 2011, 2015; Sun et al, 2015, 2019, 2021a).

Millennial-scale fluctuations co-exist with long-term orbital- and ice-volume variability; we seek to assess the potential linkages among them and in particular, the extent to which MMV is modulated by these longer-term orbital and internal climate parameters. The spectra of Ca/Ti MMV shows dominant eccentricity with less strong precession and weak obliquity variance (Fig. 2d). The spectrum of $\delta^{18}Osp$ MMV has a small peak near 100 kyr and an offset 41 kyr peak with little to no variance at the 23 kyr period (Fig. S2d). Thus, while both proxies are similarly modulated at the 100-kyr period (such that the MMV is larger during glacial intervals relative to interglacial times) the MMV modulation is variable for the two proxies at other orbital bands. As with the spectral differences in the raw records, the MMV spectra also implies different MMV modulating drivers, potentially associated with insolation, ice volume, and/or GHG for the two different archives (Friedrich et al., 2009; Thirumalai et al., 2020). How do internal and external drivers interact with each other and modulate the MMV of these records at the orbital timescale? We performed wavelet coherence and phase analyses (WTC reference here) of both MMV records relative to ETP, ice volume, $\Delta RF_{GHG}$ (the GHG radiative forcing factor, more details refer to

methods section. $CO_2$ is the main contributor and $CH_4$ contribution is less than 5%), summer insolation, and winter insolation to identify which variables might modulate the MMV of these EASM records.

The MMV in Ca/Ti is strongly coherent with ice volume and GHG at the 100,000-year earth-orbital eccentricity band and to GHG and summer insolation at the 23,000-year precession band (Figure 3c, d). $\delta^{18}$Osp MMV is most strongly coherent with GHG and ice volume at the 100-kyr band and with winter insolation at the eccentricity and obliquity band (Figure S4c, d, g).

## 4. Discussion

### Orbital-scale modulation factors for MMV of the EASM

Previous geological records and modeling indicate that high latitude ice volume or ice sheet topography plays an important role in triggering abrupt climate changes (MacAyeal, 1993; Broecker et al.,1994; Alley et al., 1999; Clark et al., 2001). In particular, abrupt climate changes are highly sensitive to ice volume variations and ice sheets are widely hypothesized to motivate and amplify these high frequency signals within a constrained benthic oxygen isotope-"ice volume threshold" between 3.5 and 4.5‰ (Wara et al., 2000; Shackleton et al., 2000; Bailey et al., 2010; Naffs et al., 2013; Zhang et al., 2014). Wavelet coherence between the MMV of loess Ca/Ti, speleothem $\delta^{18}$O and the global benthic $\delta^{18}$O stack show excellent coherence and near-zero phase with ice volume at the 100 kyr band (Fig. S3a, c and S4e, g); this demonstrates that EASM MMV primarily follows the glacial-interglacial rhythm of ice volume variations, enlarged during glacial times and dampened during interglacial times. However coherence of the MMV for these two proxies with the benthic $\delta^{18}$O stack are relatively weak and variable at the 41 kyr band ($\delta^{18}$Osp; Figure S4e,g) and 23-kyr band (Ca/Ti; Fig. S3a,c). These relationships demonstrate that ice volume directly modulates the MMV of the EASM, predominantly at the 100 kyr band, with high ice volume corresponding to larger MMV.

GHG concentration is another potential driver of abrupt climate changes (Ruddiman and Raymo, 2003; Alvarez-Solas et al., 2011; Hopcroft et al., 2014; Zhang et al., 2017).Wavelet coherence between the MMV of loess Ca/Ti, speleothem $\delta^{18}$O and the record of GHG RF show excellent coherence and ~180° phase at the 100-kyr eccentricity band (Fig. 3b, d and Fig. S4b, d) indicating strong MMV at times of low GHG. Given the coupled nature of global ice-volume and

atmospheric GHG, it is clear that over the late Pleistocene glacial-interglacial cycles, these two factors modulate the MMV of the EASM as recorded by Ca/Ti and speleothem $\delta^{18}O$ such that abrupt climate change is amplified during times of high ice volume and low GHG concentration. However, this is not the case for the precession band. MMV of loess Ca/Ti displays discrete intervals high coherence and near-zero phase with GHG RF at the precession band (Figure 3b, d), which is not the case for speleothem $\delta^{18}O$ (Figure S4b, d). Thus, GHG RF does play a role in modulating Ca/Ti MMV but not that of $\delta^{18}Osp$ at the precession band, indicating a difference in the millennial-scale response of these two proxies at this time-scale. We investigate this further by assessing the response to local insolation forcing.

The MMV of Ca/Ti show discontinuous relatively weak coherence with 35°N summer insolation at the precession band with even weaker coherence at the 41-kyr band (Figure 3a, c); we note that the summer insolation modulation is less strong relative to that of GHG at the precession band (Figure 3b, d). In contrast, the MMV of $\delta^{18}Osp$ displays high coherence and zero phase with 35°N winter insolation at 100 kyr period, relatively weaker coherence, with a lagging phase, at the 41 kyr band, and negligible coherence at the 23-ky band (Figure S4a, c). These results indicate that the MMV of speleothem $\delta^{18}O$ is modulated by local winter insolation, opposite to the Cheng et al., (2016) hypothesis calling on north hemisphere summer insolation.

**Mechanism and implication for modulation of EASM MMV**

At glacial-interglacial time scales, the MMV is amplified under the glacial boundary conditions. These millennial-scale variability recorded in loess and cave records is thought dynamic linked with high latitude North Atlantic Heinrich and DO events (Cheng et al., 2009, 2016; Sun et al., 2012, 2021a, b). They are thought to be controlled by ice volume and freshwater perturbation / Northern Hemisphere ice sheet changes, respectively and associated with Atlantic meridional overturning circulation (AMOC) changes (McManus et al., 1999; Hemming, 2004; Hodell et al., 2008; Naffs et al., 2013; Zhang et al., 2013; Menviel et al., 2014). At the intermediate heights (volume) of the ice sheets, minor changes in the height of Northern Hemisphere ice sheet and atmospheric $CO_2$ concentrations can trigger the rapid climate transitions (Zhang et al., 2014, 2017). Altering the height of Northern Hemisphere ice sheets (NHISs) lead to changes in the gyre circulation and sea-ice coverage by shifting the Northern westerlies (Zhang et al., 2014). The maximum westerly wind stress shifts northwards associated with gradual increase of the Northern

Hemisphere ice volume. This, in turn, encourages the EAM move northward and results in increases in the MMV of EASM rainfall (especially northern China). In addition, $CO_2$ is supposed to act as an internal feedback agent to AMOC changes (Baker et al., 2007, 2016). Under intermediate glacial condition, when the AMCO reaches a regime of bi-stability, rising $CO_2$ during Heinrich Stadial cold events can trigger abrupt transitions to warm conditions. Decreasing $CO_2$ during warm events leads to abrupt cooling transitions (Zhang et al., 2017). Therefore, $CO_2$ generally provides a negative feedback on MMV of EASM rainfall. During interglacial times, decreasing ice volume, accompanied by reduced sea ice and stronger freshwater perturbation, is correlated with lower frequency and smaller amplitude variability. The increasing GHG concentrations in atmosphere would further alter the sea surface temperature by greenhouse effect and then modulate the MMV sequentially.

At the precession band, higher GHG concentration and local insolation correspond to larger MMV of subtropical rainfall. Recent transient sensitivity experiments of $\delta^{18}$Osp suggests that millennial-scale rainfall variability is driven primarily by meltwater and secondarily by insolation (He et al., 2021). During interglacial times under the combined influence of insolation and $CO_2$, model simulation shows that when insolation reaches the lower "threshold" value (358.2 and 352.1 W. $m^{-2}$), it triggers a strong abrupt weakening of the AMOC and results in abrupt cooling transitions over last 800ka (Yin et al., 2021). Increased insolation could warm sea surface temperature and accelerate freshwater input from high latitude ice sheet as well as altering GHG concentration in the atmosphere (Lewkowicz and Way, 2019; Zheng et al., 2020), which could, in turn, modulate MMV changes in the low latitude monsoon regions.

If both millennial-scale Ca/Ti and $\delta^{18}$Osp represent subtropical rainfall amount, the modulation factors should be consistent. However, eccentricity, obliquity and precession bands MMV modulators differ for loess Ca/Ti and $\delta^{18}$Osp, indicating they monitor different aspects of millennial-scale monsoon circulations. Modern observations and Lagrangian trajectories of air parcels in China during the summer monsoon indicate that moisture-induced precipitation doesn't derive from the strongest water vapor pathways (Sun et al., 2011; Jiang et al., 2017); local water vapor recycling contributes significantly to regional precipitation in East China (over 30%) and North China (exceeding 55%) (Shi et al., 2020). Hence, we speculate that $\delta^{18}$Osp MMV monitors changes in the isotopic composition of rainfall, varying with changes in westerly transport paths

266 associated with North Atlantic cooling events, consistent with the MMV of $\delta^{18}$Osp being closely
267 linkage to winter insolation at 100- and 41- kyr periods and the absence of MMV modulation at
268 precession band. We further hypothesize that Ca/Ti mainly represents the MMV in local rainfall
269 amount, consistent with the MMV of tropical rainfall being more dynamically related to GHG and
270 summer insolation at precession band.

271 In recent decades atmospheric GHG concentration is accelerating due to anthropogenic
272 contribution of fossil fuels suggesting that EASM (extreme) precipitation will increase as well.
273 This inference is consistent with model simulations indicating that the number of extreme daily
274 precipitation events and mean precipitation overall will increase significantly in response to higher
275 GHG concentration (Dairaku and Emori, 2006; Li et al., 2015; Li and Ting, 2017). The
276 anthropogenic GHG-evoked warming is projected to increase the lower-tropospheric water vapor
277 content and enhance the thermal contrast between land and ocean (Kitoh et al., 1997; Hu et al.,
278 2000; Ashrit et al., 2003). This will give rise to a northward shift of lower tropospheric monsoon
279 circulation and an increase rainfall during the East Asian summer monsoon (Vecchi and Soden,
280 2007; Held and Soden 2006). Our results indicate that factors modulating EASM precipitation
281 MMV in the past are consistent with those predicted to influence future changes in monsoonal
282 precipitation, lending further confidence in those projections.

283 **5. Summary**

284 Our high-resolution loess Ca/Ti record displays millennial monsoon oscillations were
285 persistent over the last 650 kyr. Wavelet results highlights the remarkable GHG modulation at both
286 100 kyr and precession band as well as ice volume at 100 kyr period and local insolation forcing at
287 precession band. The MMV of loess Ca/Ti and speleothem $\delta^{18}$O are modulated by different orbital
288 factors, implying that these two proxies document different climatic response of millennial-scale
289 monsoon circulations. The underlying dynamics on how these internal and external factors
290 modulate the MMV still needs further model testing. In recent decades, atmospheric GHG
291 concentration is dramatically increasing due to anthropogenic contribution of fossil fuels
292 (Bousquet et al., 2006; Davis et al., 2010), resulting in accelerated melting of ice-sheets in bi-polar
293 regions (Swingedouw et al., 2008; Pattyn et al., 2018; Golledge et al., 2019). Their combined
294 effects lead to more frequently occurrence of extreme rainfall ( Dairaku and Emori, 2006; Li et al.,
295 2015; Li and Ting, 2017; IPCC, 2018). Our results indicate that the MMV EASM rainfall can be

296 modulated by ice volume, GHG, and insolation factors, consistent with those predictions to
297 influence future changes in monsoonal precipitation.
298
299 **Acknowledgments**
300 We thank Xiaojing Du for offering idea on potential model test for this paper. This work was
301 supported by grants from the Strategic Leading Research Program of Chinese Academy of Science
302 (XDB40000000) and National Natural Science Foundation of China (41525008 and 41977173).
303 Loess Ca/Ti of this research is temporarily available as a supporting information file.
304

305 ## Declaration of Competing Interest

306 The authors declare that they have no known competing financial interests or personal
307 relationships that could have appeared to influence the work reported in this paper.
308

309 ## References

310 Alvarez-Solas, J., Charbit, S., Ramstein, G., Paillard, D., Dumas, C., Ritz, C., & Roche, D. M.
311 (2011). Millennial-scale oscillations in the Southern Ocean in response to atmospheric $CO_2$
312 increase. Global and Planetary Change, 76(3-4), 128-136.
313 https://doi.org/10.1016/j.gloplacha.2010.12.004
314 An, Z., Liu, T., Lu, Y., Porter, S.C., Kukla, G., Wu, X., & Hua, Y., (1990). The long-term
315 paleomonsoon variation recorded by the loess-paleosol sequence in central China. Quaternary
316 International, 7, 91-95. https://doi.org/10.1016/1040-6182(90)90042-3
317 An, Z. (2000). The history and variability of the East Asian paleomonsoon climate. Quaternary
318 Science Reviews, 19(1-5), 171-187. https://doi.org/10.1016/S0277-3791(99)00060-8
319 An, Z., Clemens, S.C., Shen, J., Qiang, X., Jin, Z., Sun, Y., Prell, W. L., Luo, J., Wang, S., Xu, H.,
320 Cai, Y., Zhou, W., Liu, X., Liu, W., Shi, Z., Yan, L., Xiao, X., Chang, H., Wu, F., Ai., L., & Lu,
321 F. (2011). Glacial-interglacial Indian summer monsoon dynamics. Science, 333(6043), 719-723.
322 https://doi.org/10.1126/science.1203752
323 An, Z., Wu, G., Li, L., Li, J., Sun, Y., Liu, Y., Zhou, W., Cai, Y., Duan, A., Li, L., Mao, J.,Cheng,
324 H., Shi, Z., Tan, L., Yan, H., Ao, H., Chang, H., & Feng, J. (2015). Global monsoon dynamics
325 and climate change. Annual review of earth and planetary sciences, 43, 29-77.
326 https://doi.org/10.1146/annurev-earth-060313-054623
327 Alley, R. B., Clark, P. U., Keigwin, L. D., & Webb, R. S. (1999). Making sense of millennial-scale
328 climate change. Geophysical Monograph-American Geophysical Union, 112, 385-394.

https://doi.org/10.1029/GM112p0385

Ashrit, R. G., Douville, H., & Kumar, K. R. (2003). Response of the Indian monsoon and ENSO-monsoon teleconnection to enhanced greenhouse effect in the CNRM coupled model. Journal of the Meteorological Society of Japan. Ser. II, 81(4), 779-803. https://doi.org/10.2151/jmsj.81.779

Bailey, I., Bolton, C. T., DeConto, R. M., Pollard, D., Schiebel, R., & Wilson, P. A. (2010). A low threshold for North Atlantic ice rafting from "low‐slung slippery" late Pliocene ice sheets. Paleoceanography, 25(1). https://doi.org/10.1029/2009PA001736

Barker, S., & Knorr, G. (2016). A paleo-perspective on the AMOC as a tipping element. PAGES Magazine, 24(1), 14-15. http://orca.cardiff.ac.uk/id/eprint/95186

Barker, S., & Knorr, G. (2007). Antarctic climate signature in the Greenland ice core record. Proceedings of the National Academy of Sciences, 104(44), 17278-17282. https://doi.org/10.1073/pnas.0708494104

Barker, S., Knorr, G., Edwards, R. L., Parrenin, F., Putnam, A. E., Skinner, L. C., Wolff, E. & Ziegler, M. (2011). 800,000 years of abrupt climate variability. Science, 334(6054), 347-351. https://doi.org/10.1126/science.1203580

Bond, G., Broecker, W., Johnsen, S., McManus, J., Labeyrie, L., Jouzel, J., & Bonani, G. (1993). Correlations between climate records from North Atlantic sediments and Greenland ice. Nature, 365(6442), 143-147. https://doi.org/10.1038/365143a0

Bond, G., Heinrich, H., Broecker, W., Labeyrie, L., McManus, J., Andrews, J., Huon, S., Jantschik, R., Clasen, S., Simet, C., Tedesco, K., Klas, M., Bonani, G., & Ivy, S. (1992). Evidence for massive discharges of icebergs into the North Atlantic ocean during the last glacial period. Nature, 360(6401), 245-249. https://doi.org/10.1038/360245a0

Bousquet, P., Ciais, P., Miller, J. B., Dlugokencky, E. J., Hauglustaine, D. A., Prigent, C., & White, J. (2006). Contribution of anthropogenic and natural sources to atmospheric methane variability. Nature, 443(7110), 439-443. https://doi.org/10.1038/nature05132

Broecker, W. S. (1994). Massive iceberg discharges as triggers for global climate change. Nature, 372(6505), 421-424. https://doi.org/10.1038/372421a0

Cheng, H., Edwards, R.L., Broecker, W.S., Denton, G.H., Kong, X., Wang, Y., Zhang, R., &Wang, X. (2009). Ice age terminations. Science, 326(5950), 248-252. https://doi.org/10.1126/science.1177840

Cheng, H., Edwards, L., Sinha, A., Spötl, C., Yi, L., Chen, S., Kelly, M., Kathayat, G., Wang,X.F., Li, X.L., Kong, X.G., Wang, Y.J., Ning, Y.F., Zhang, H.W. (2016). The Asian monsoon over the past 640,000 years and ice age terminations. Nature, 534(7609), 640-646. https://doi.org/10.1038/nature18591

Clark, P. U., Marshall, S. J., Clarke, G. K., Hostetler, S. W., Licciardi, J. M., & Teller, J. T., (2001). Freshwater forcing of abrupt climate change during the last glaciation. Science, 293(5528), 283-287. https://doi.org/10.1126/science.1062517

Clemens, S. C., Holbourn, A., Kubota, Y., Lee, K. E., Liu, Z., Chen, G., Nelson, A., Fox-Kemper, B. (2018). Precession-band variance missing from East Asian monsoon runoff. Nature communications, 9(1), 1-12. https://doi.org/10.1038/s41467-018-05814-0

Clemens, S. C., Prell, W. L., & Sun, Y. (2010). Orbital - scale timing and mechanisms driving Late Pleistocene Indo-Asian summer monsoons: Reinterpreting cave speleothem δ 18O. Paleoceanography, 25(4). https://doi.org/10.1029/2010PA001926

Cook, E. R., Anchukaitis, K. J., Buckley, B. M., D'Arrigo, R. D., Jacoby, G. C., & Wright, W. E. (2010). Asian monsoon failure and megadrought during the last millennium. Science, 328(5977), 486-489. https://doi.org/10.1126/science.1185188

Dansgaard, W., Clausen, H. B., Gundestrup, N., Hammer, C. U., Johnsen, S. F., Kristinsdottir, P. M., & Reeh, N. (1982). A new Greenland deep ice core. Science, 218(4579), 1273-1277. https://doi.org/10.1126/science.218.4579.1273

Dansgaard, W., Johnsen, S. J., Clausen, H. B., Dahl-Jensen, D., Gundestrup, N. S., Hammer, C. U., & Bond, G. (1993). Evidence for general instability of past climate from a 250-kyr ice-core record. Nature, 364(6434), 218-220. https://doi.org/10.1038/364218a0

Dairaku, K., & Emori, S. (2006). Dynamic and thermodynamic influences on intensified daily rainfall during the Asian summer monsoon under doubled atmospheric $CO_2$ conditions. Geophysical Research Letters, 33(1). https://doi.org/10.1029/2005GL024754

Davis, S. J., Caldeira, K., & Matthews, H. D. (2010). Future $CO_2$ emissions and climate change from existing energy infrastructure. Science, 329(5997), 1330-1333. https://doi.org/10.1126/science.1188566

Ding, Z.L., Sun, J., Rutter, N.W., Rokosh, D., & Liu, T. (1999). Changes in sand content of loess deposits along a north-south transect of the Chinese Loess Plateau and the implications for desert variations. Quaternary Research, 52(1), 56-62. https://doi.org/10.1006/qres.1999.2045

Ding, Y., H., & Chan, J. (2005). The East Asian summer monsoon: an overview. Meteorology and Atmospheric Physics, 89(1), 117-142. https://doi.org/10.1007/s00703-005-0125-z

Friedrich, T., Timmermann, A., Timm, O., Mouchet, A., & Roche, D. M. (2009). Orbital modulation of millennial-scale climate variability in an earth system model of intermediate complexity. Climate of the Past Discussions, 5(4), 2019-2051. https://doi.org/10.5194/cpd-5-2019-2009

Golledge, N. R., Keller, E. D., Gomez, N., Naughten, K. A., Bernales, J., Trusel, L. D., & Edwards, T. L. (2019). Global environmental consequences of twenty-first-century ice-sheet melt. Nature, 566(7742), 65-72. https://doi.org/10.1038/s41586-019-0889-9

Grinsted, A., Moore, J. C., & Jevrejeva, S. (2004). Application of the cross wavelet transform and wavelet coherence to geophysical time series. Nonlinear processes in geophysics, 11(5/6), 561-566. https://doi.org/10.5194/npg-11-561-2004

Guo, F., Clemens, S. C., Wang, T., Wang, Y., Liu, Y., Wu, F., Jin, Z., & Sun, Y. (2021). Monsoon variations inferred from high-resolution geochemical records of the Linxia loess/paleosol

405 sequence, western Chinese Loess Plateau. Catena, 198, 105019.
406 https://doi.org/10.1016/j.catena.2020.105019
407 Guo, Z., Liu, T., Guiot, J., Wu, N., Lü, H., Han, J., Gu, Z. (1996). High frequency pulses of East
408 Asian monsoon climate in the last two glaciations: link with the North Atlantic. Climate
409 Dynamics, 12(10), 701-709. https://doi.org/10.1007/s003820050137
410 Guo, Z., Zhou, X., & Wu, H. (2012). Glacial-interglacial water cycle, global monsoon and
411 atmospheric methane changes. Climate Dynamics, 39(5), 1073-1092.
412 https://doi.org/10.1007/s00382-011-1147-5
413 He, C., Liu, Z., Otto-Bliesner, B.L., Brady, E.C., Zhu, C., Tomas, R., Clark, P.U., Zhu, J., Jahn, A.,
414 Gu, S., Zhang, J., Nusbaumer, J., Noone, D., Cheng, H., Wang, Y., Yan, M., & Bao, Y. (2021).
415 Hydroclimate footprint of pan-Asian monsoon water isotope during the last deglaciation.
416 Science Advances, 7(4), eabe2611. https://doi.org/10.1126/sciadv.abe2611
417 Heinrich, H. (1988). Origin and consequences of cyclic ice rafting in the northeast Atlantic Ocean
418 during the past 130,000 years, Quaternary research, 29(2), 142-152.
419 https://doi.org/10.1016/0033-5894(88)90057-9
420 Held, I. M., & Soden, B. J. (2006). Robust responses of the hydrological cycle to global warming.
421 Journal of climate, 19(21), 5686-5699. https://doi.org/10.1175/JCLI3990.1
422 Hemming, S. R. (2004). Heinrich events: Massive late Pleistocene detritus layers of the North
423 Atlantic and their global climate imprint. Reviews of Geophysics, 42(1).
424 https://doi.org/10.1029/2003RG000128
425 Hodell, D. A., Channell, J. E., Curtis, J. H., Romero, O. E., & Röhl, U. (2008). Onset of "Hudson
426 Strait" Heinrich events in the eastern North Atlantic at the end of the middle Pleistocene
427 transition (~ 640 ka)?. Paleoceanography, 23(4). https://doi.org/10.1029/2008PA001591
428 Hoegh-Guldberg, O., Jacob, D., Bindi, M., et al,. (2018). Impacts of 1.5 C global warming on
429 natural and human systems. Global warming of 1.5 C. An IPCC Special Report. IPCC
430 Secretariat, 175-311. http://hdl.handle.net/10138/311749
431 Hopcroft, P. O., Valdes, P. J., Wania, R., & Beerling, D. J. (2014). Limited response of peatland
432 $CH_4$ emissions to abrupt Atlantic Ocean circulation changes in glacial climates. Climate of the
433 Past, 10(1), 137-154. https://doi.org/10.5194/cp-10-137-2014
434 Huang, R., Chen, J., & Huang, G. (2007). Characteristics and variations of the East Asian
435 monsoon system and its impacts on climate disasters in China. Advances in Atmospheric
436 Sciences, 24(6), 993-1023. https://doi.org/10.1007/s00376-007-0993-x
437 Huang, R., Liu, Y., Du, Z., Chen, J., & Huangfu, J. (2017). Differences and links between the East
438 Asian and South Asian summer monsoon systems: Characteristics and variability. Advances in
439 Atmospheric Sciences, 34(10), 1204-1218. https://doi.org/10.1007/s00376-017-7008-3
440 Hu, Z. Z., Latif, M., Roeckner, E., & Bengtsson, L. (2000). Intensified Asian summer monsoon
441 and its variability in a coupled model forced by increasing greenhouse gas concentrations.
442 Geophysical Research Letters, 27(17), 2681-2684. https://doi.org/10.1029/2000GL011550

Jiang, Z., Jiang, S., Shi, Y., Liu, Z., Li, W., & Li, L. (2017). Impact of moisture source variation on decadal - scale changes of precipitation in North China from 1951 to 2010. Journal of Geophysical Research: Atmospheres, 122(2), 600-613. https://doi.org/10.1002/2016JD025795

Kitoh, A., Yukimoto, S., Noda, A., & Motoi, T. (1997). Simulated changes in the Asian summer monsoon at times of increased atmospheric $CO_2$. Journal of the Meteorological Society of Japan. Ser. II, 75(6), 1019-1031. https://doi.org/10.2151/jmsj1965.75.6_1019

Lai, Z. P., & Wintle, A. G. (2006). Locating the boundary between the Pleistocene and the Holocene in Chinese loess using luminescence. The Holocene, 16(6), 893-899. https://doi.org/10.1191/0959683606hol980rr

Lai, Z., Wintle, A. G., & Thomas, D. S. (2007). Rates of dust deposition between 50 ka and 20 ka revealed by OSL dating at Yuanbao on the Chinese Loess Plateau. Palaeogeography, Palaeoclimatology, Palaeoecology, 248(3-4), 431-439. https://doi.org/10.1016/j.palaeo.2006.12.013

Lewkowicz, A. G., & Way, R. G. (2019). Extremes of summer climate trigger thousands of thermokarst landslides in a High Arctic environment. Nature communications, 10(1), 1-11. https://doi.org/10.1038/s41467-019-09314-7

Li, F. X., Zhang, S. Y., Chen, D., He, L., & Gu, L. L. (2017). Inter-decadal variability of the east Asian summer monsoon and its impact on hydrologic variables in the Haihe River Basin. China, J. Resour. Ecol, 8(2), 174-375. https://doi.org/10.5814/j.issn.1674-764X.2017.02.008

Li, X., & Ting, M. (2017). Understanding the Asian summer monsoon response to greenhouse warming: The relative roles of direct radiative forcing and sea surface temperature change. Climate Dynamics, 49(7), 2863-2880. https://doi.org/10.1007/s00382-016-3470-3

Li, X., Ting, M., Li, C., & Henderson, N. (2015). Mechanisms of Asian summer monsoon changes in response to anthropogenic forcing in CMIP5 models. Journal of Climate, 28(10), 4107-4125. https://doi.org/10.1175/JCLI-D-14-00559.1

Lisiecki, L. E., & Raymo, M. E. (2005). A Pliocene-Pleistocene stack of 57 globally distributed benthic $\delta^{18}O$ records. Paleoceanography, 20(1). https://doi.org/10.1029/2004PA001071

Liu, J., Wang, B., Cane, M. A., Yim, S. Y., & Lee, J. Y. (2013). Divergent global precipitation changes induced by natural versus anthropogenic forcing. Nature, 493(7434), 656-659. https://doi.org/10.1038/nature11784

MacAyeal, D. R. (1993). Binge/purge oscillations of the Laurentide Ice Sheet as a cause of the North Atlantic's Heinrich events, Paleoceanography 8(6), 775-784. https://doi.org/10.1029/93PA02200

McManus, J. F., Oppo, D. W., & Cullen, J. L. (1999). A 0.5-million-year record of millennial-scale climate variability in the North Atlantic. science, 283(5404), 971-975. https://doi.org/10.1126/science.283.5404.971

Menviel, L., Timmermann, A., Friedrich, T., & England, M. H. (2014). Hindcasting the continuum of Dansgaard-Oeschger variability: mechanisms, patterns and timing. Climate of the Past, 10(1),

481 63-77. https://doi.org/10.5194/cp-10-63-2014
482 Naafs, B. D. A., Hefter, J., & Stein, R. (2013). Millennial-scale ice rafting events and Hudson
483 Strait Heinrich (-like) Events during the late Pliocene and Pleistocene: a review. Quaternary
484 Science Reviews, 80, 1-28. https://doi.org/10.1016/j.quascirev.2013.08.014
485 Pattyn, F., Ritz, C., Hanna, E., Asay-Davis, X., DeConto, R., Durand, G., & Van den Broeke, M.,
486 (2018). The Greenland and Antarctic ice sheets under 1.5 C global warming. Nature Climate
487 Change, 8(12), 1053-1061. https://doi.org/10.1038/s41558-018-0305-8
488 Porter, S. C., & Zhisheng, A. (1995). Correlation between climate events in the North Atlantic and
489 China during the last glaciation. Nature, 375(6529), 305-308. https://doi.org/10.1038/375305a0
490 Ramaswamy, V. et al. Radiative forcing of climate change in Climate Change 2001: The Scientific
491 Basis, Houghton, J. T. et al. eds, Cambridge University Press, 349-416.
492 Rao, Z., Chen, F., Cheng, H., Liu, W., Lai, Z., & Bloemendal, J. (2013). High-resolution summer
493 precipitation variations in the western Chinese Loess Plateau during the last glacial. Scientific
494 Reports, 3(1), 1-6. https://doi.org/10.1038/srep02785
495 Ruddiman, W. F., & Raymo, M. E. (2003). A methane-based time scale for Vostok ice. Quaternary
496 Science Reviews, 22(2-4), 141-155. https://doi.org/10.1016/S0277-3791(02)00082-3
497 Shackleton, N. J., Hall, M. A., & Vincent, E. (2000). Phase relationships between millennial ‐
498 scale events 64,000-24,000 years ago. Paleoceanography, 15(6), 565-569.
499 https://doi.org/10.1029/2000PA000513
500 Shi, Y., Jiang, Z., Liu, Z., & Li, L. (2020). A Lagrangian analysis of water vapor sources and
501 pathways for precipitation in East China in different stages of the East Asian summer monsoon.
502 Journal of Climate, 33(3), 977-992. https://doi.org/10.1175/JCLI-D-19-0089.1
503 Sun, B., Zhu, Y., & Wang, H. (2011). The recent interdecadal and interannual variation of water
504 vapor transport over eastern China. Advances in Atmospheric Sciences, 28(5), 1039-1048.
505 https://doi.org/10.1007/s00376-010-0093-1
506 Sun, Y., Clemens, S. C., An, Z., & Yu, Z. (2006). Astronomical timescale and palaeoclimatic
507 implication of stacked 3.6-Myr monsoon records from the Chinese Loess Plateau. Quaternary
508 Science Reviews, 25(1-2), 33-48. https://doi.org/10.1016/j.quascirev.2005.07.005
509 Sun, Y., Clemens, S., Guo, F., Liu, X., Wang, Y., Yan, Y., & Liang, L. (2021).
510 High-sedimentation-rate loess records: A new window into understanding orbital-and
511 millennial-scale monsoon variability. Earth-Science Reviews, 103731.
512 https://doi.org/10.1016/j.earscirev.2021.103731
513 Sun, Y., Clemens, S. C., Morrill, C., Lin, X., Wang, X., & An, Z. (2012). Influence of Atlantic
514 meridional overturning circulation on the East Asian winter monsoon. Nature Geoscience, 5(1),
515 46-49. https://doi.org/10.1038/ngeo1326
516 Sun, Y., Kutzbach, J., An, Z., Clemens, S., Liu, Z., Liu, W., ... & Li, Y. (2015). Astronomical and
517 glacial forcing of East Asian summer monsoon variability. Quaternary Science Reviews, 115,
518 132-142. https://doi.org/10.1016/j.quascirev.2015.03.009

519 Sun, Y., Liang, L., Bloemendal, J., Li, Y., Wu, F., Yao, Z., & Liu, Y. (2016). High-resolution
520 scanning XRF investigation of Chinese loess and its implications for millennial-scale monsoon
521 variability. Journal of Quaternary Science, 31(3), 191-202. https://doi.org/10.1002/jqs.2856
522 Sun, Y., Yin, Q., Crucifix, M., Clemens, C., Araya-Melo, P., Liu, W., Qiang, X., Liu, Q.,Zhao, H.,
523 Liang, L., Chen, H., Li, Y., Zhang, L., Dong, G., Li, M., Zhou, W., Berger, A.,& An, Z. (2019).
524 Diverse manifestations of the mid-Pleistocene climate transition. Nature communications, 10(1),
525 1-11. https://doi.org/10.1038/s41467-018-08257-9
526 Swingedouw, D., Fichefet, T., Huybrechts, P., Goosse, H., Driesschaert, E., & Loutre, M. F. (2008).
527 Antarctic ice-sheet melting provides negative feedbacks on future climate warming.
528 Geophysical Research Letters, 35(17). https://doi.org/10.1029/2008GL034410
529 Thirumalai, K., Clemens, S. C., & Partin, J. W. (2020). Methane, Monsoons, and Modulation of
530 Millennial-Scale Climate. Geophysical Research Letters, 47(9), e2020GL087613.
531 https://doi.org/10.1029/2020GL087613
532 Vecchi, G. A., & Soden, B. J. (2007). Global warming and the weakening of the tropical
533 circulation. Journal of Climate, 20(17), 4316-4340. https://doi.org/10.1175/JCLI4258.1
534 VanderPlas, J. T. (2018). Understanding the lomb-scargle periodogram. The Astrophysical Journal
535 Supplement Series, 236(1), 16. https://doi.org/10.3847/1538-4365/aab766
536 Wang, B., & Ding, Q. (2008). Global monsoon: Dominant mode of annual variation in the tropics.
537 Dynamics of Atmospheres and Oceans, 44(3-4), 165-183.
538 https://doi.org/10.1016/j.dynatmoce.2007.05.002
539 Wang, P. (2009). Global monsoon in a geological perspective. Chinese Science Bulletin, 54(7),
540 1113-1136. https://doi.org/10.1007/s11434-009-0169-4
541 Wara, M. W., Ravelo, A. C., Revenaugh, J. S., 2000. The pacemaker always rings twice.
542 Paleoceanography 15(6), 616-624. https://doi.org/10.1029/2000PA000500
543 Webster, P. J., Magana, V. O., Palmer, T. N., Shukla, J., Tomas, R. A., Yanai, M. U., & Yasunari, T.
544 (1998). Monsoons: Processes, predictability, and the prospects for prediction. Journal of
545 Geophysical Research: Oceans, 103(C7), 14451-14510. https://doi.org/10.1029/97JC02719
546 Wang, Y. J., Cheng, H., Edwards, R. L., An, Z. S., Wu, J. Y., Shen, C. C., & Dorale, J. A. (2001). A
547 high-resolution absolute-dated late Pleistocene monsoon record from Hulu Cave, China.
548 Science, 294(5550), 2345-2348. https://doi.org/10.1126/science.1064618
549 Wang, Y., Cheng, H., Edwards, R. L., Kong, X., Shao, X., Chen, S., & An, Z. (2008).
550 Millennial-and orbital-scale changes in the East Asian monsoon over the past 224,000 years.
551 Nature, 451(7182), 1090-1093. https://doi.org/10.1038/nature06692
552 Wang, Y., Guo, F., Ma, L., Yan, Y., Liu, X., & Sun, Y. (2020). Millennial-scale summer monsoon
553 oscillations over the last 260 ka revealed by high-resolution elemental results of the Mangshan
554 loess-palaeosol sequence from the southeastern Chinese Loess Plateau. Quaternary International,
555 552, 164-174. https://doi.org/10.1016/j.quaint.2020.05.039
556 Wu, S., Hu, Z., Wang, Z., Cao, S., Yang, Y., Qu, X., & Zhao, W. (2021). Spatiotemporal variations

in extreme precipitation on the middle and lower reaches of the Yangtze River Basin (1970–2018). Quaternary International, 592, 80-96. https://doi.org/10.1016/j.quaint.2021.04.010

Yang, S., & Ding, Z. (2014). A 249 kyr stack of eight loess grain size records from northern China documenting millennial-scale climate variability. Geochemistry, Geophysics, Geosystems, 15(3), 798-814. https://doi.org/10.1002/2013GC005113

Yancheva, G., Nowaczyk, N.R., Mingram, J., Dulski, P., Schettler, G., Negendank, J.F.W.,Liu, J., Sigman, D.M., Peterson, L.C., & Haug, G. H. (2007). Influence of the intertropical convergence zone on the East Asian monsoon. Nature, 445(7123), 74-77. https://doi.org/10.1038/nature05431

Yin, Q. Z., Wu, Z. P., Berger, A., Goosse, H., & Hodell, D. (2021). Insolation triggered abrupt weakening of Atlantic circulation at the end of interglacials. Science, 373(6558), 1035-1040. https://doi.org/10.1126/science.abg1737

Zhang, H., Griffiths, M. L., Chiang, J. C. H., Kong, W., Wu, S., Atwood, A., Huang, J., Cheng, H., Ning, Y., & Xie, S. (2018). East Asian hydroclimate modulated by the position of the westerlies during Termination I. Science, 362(6414), 580-583. https://doi.org/10.1126/science.aat9393

Zhang, X., Knorr, G., Lohmann, G., & Barker, S. (2017). Abrupt North Atlantic circulation changes in response to gradual $CO_2$ forcing in a glacial climate state. Nature Geoscience, 10(7), 518-523. https://doi.org/10.1038/ngeo2974

Zhang, X., Lohmann, G., Knorr, G., & Purcell, C. (2014). Abrupt glacial climate shifts controlled by ice sheet changes. Nature, 512(7514), 290-294. https://doi.org/10.1038/nature13592

Zhang, X., Lohmann, G., Knorr, G., & Xu, X. (2013). Different ocean states and transient characteristics in Last Glacial Maximum simulations and implications for deglaciation. Climate of the Past, 9(5), 2319-2333. https://doi.org/10.5194/cp-9-2319-2013

Zheng, Y., Fang, Z., Fan, T., Liu, Z., Wang, Z., Li, Q., Pancost, R., & Naafs, B. D. A. (2020). Operation of the boreal peatland methane cycle across the past 16 ky. Geology, 48(1), 82-86. https://doi.org/10.1130/G46709.1

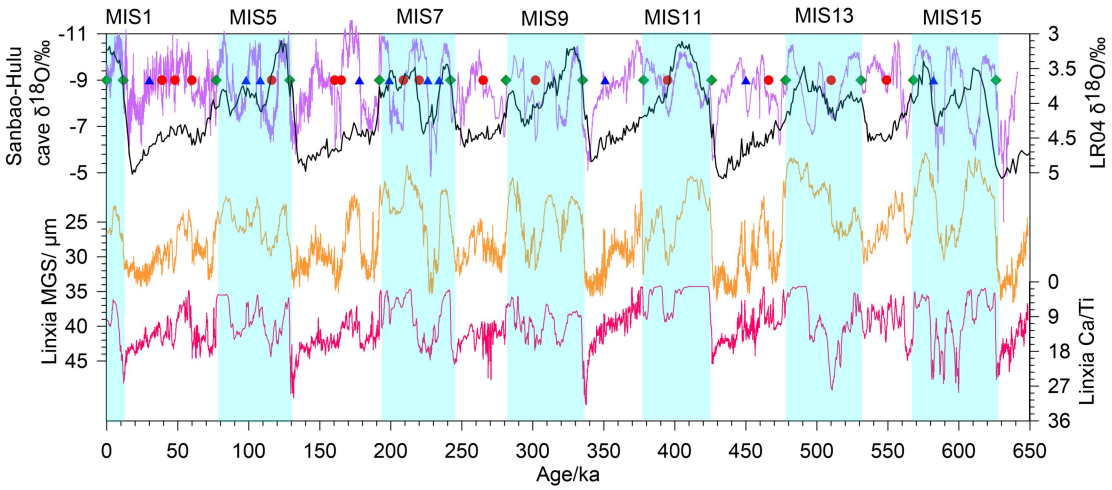


584

585 Fig. 1 Variations of mean grain size, Ca/Ti over last 650 ka and age model of Linxia loess section.
586 Comparison of mean grain size and Ca/Ti in Linxia section with Sanbao-Hulu (Cheng et al., 2009,
587 2016) and benthic $\delta^{18}O$ stack (Lisiecki and Raymo, 2005). The dark brown squares, blue triangles
588 and red dots represent the first (glacial-interglacial transition), second (precession cycles) and third
589 (millennial-scale events) class age control points at the corresponding position of cave record,
590 respectively (Sun et al., 2021). Light blue bands donate the interglacial times.

591

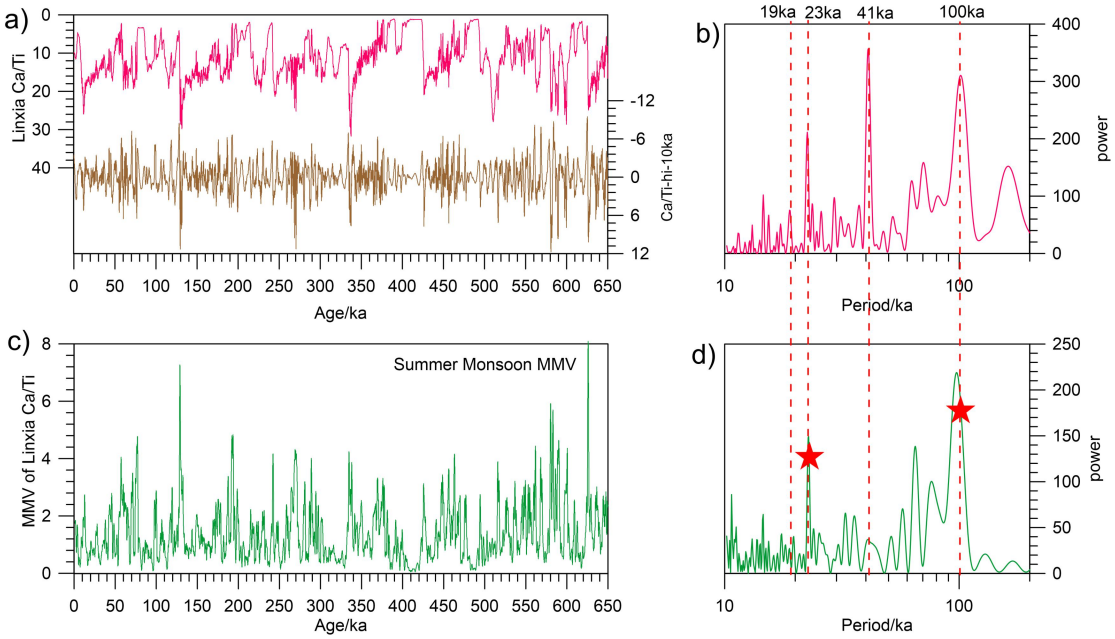


Fig.2 Raw datasets, millennial-scale components (10ka high pass filtering signals) and MMV of the Linxia loess Ca/Ti record over the past 650 ka with their corresponding spectra . The orbital bands are marked with red dashed lines (eccentricity-100 ka, obliquity-41 ka ,precession-23 ka and 19 ka). Clearly variable eccentricity, obliquity and precession variances as well as persistent millennial-scale components are observed for loess Ca/Ti.

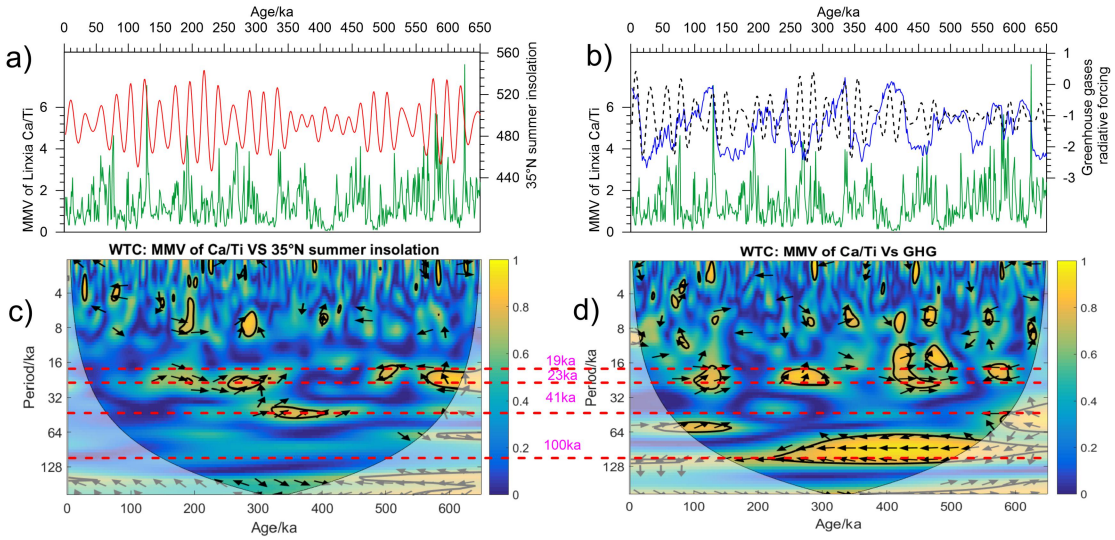


Fig. 3 Comparison of a) 35°N summer insolation and b) GHG radiative forcing (black dashed line donates the precession band-pass filtering results of GHG) for MMV of Linxia loess Ca/Ti; Wavelet coherence between c) 35°N summer insolation, d) GHG concentration and MMV of loess Ca/Ti over the past 650 ka. The orbital bands are marked with red dashed lines (eccentricity-100 kyr, obliquity-41 kyr , precession-23 kyr and 19 kyr). The black outlines indicate coefficients of determination greater than 0.76. The black arrows represent the phrase relationship with rightward, upward and downward arrows indicating in-phase, leading and lagging phase, respectively. Strong eccentricity- and precession-band GHG modulation as well as weak summer insolation forcing are observed for MMV of loess Ca/Ti.

Supporting Information for

# Greenhouse gases modulate strength of millennial subtropical rainfall and future forecasts

Fei Guo[1,2,*], Steven C. Clemens[2,*], Yuming Liu[1,3], Ting Wang[1,3], Huimin Fan[1], Xingxing Liu[1], Youbin Sun[1,4,5]

[1]State Key Laboratory of Loess and Quaternary Geology, Institute of Earth Environment, Chinese Academy of Sciences, Xian 710061, China.

[2]Department of Earth, Environmental, and Planetary Sciences, Brown University, Providence, RI 02912-1846, USA

[3]University of Chinese Academy of Sciences, Beijing 100049, China

[4]CAS Center for Excellence in Quaternary Science and Global Change, Xian 710061, China.

[5]Open Studio for Oceanic-Continental Climate and Environment Changes, Pilot National Laboratory for Marine Science and Technology (Qingdao), Qingdao 266200, China.

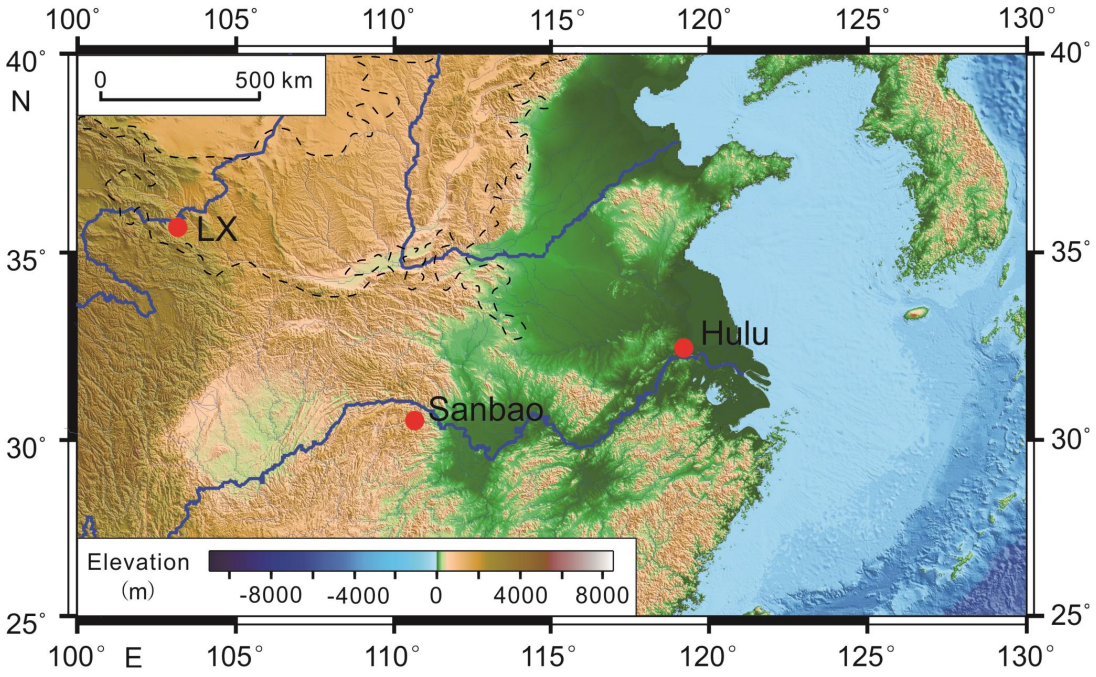


Fig. S1 The location of the Linxia (LX) loess profile and Hulu-Sanbao cave records. The Linxia profile, located on the edge of convergence zone for of alpine Qinghai-Tibet Plateau, northwest arid and the southeast monsoon area, is very sensitive to the migration of desert regions and monsoon rainfall. Sanbao-Hulu cave is located in monsoon-influenced Yangtze River Valley, sensitive to the monsoon-induced precipitation changes. Black dash line represents the scope of Chinese Loess Plateau.

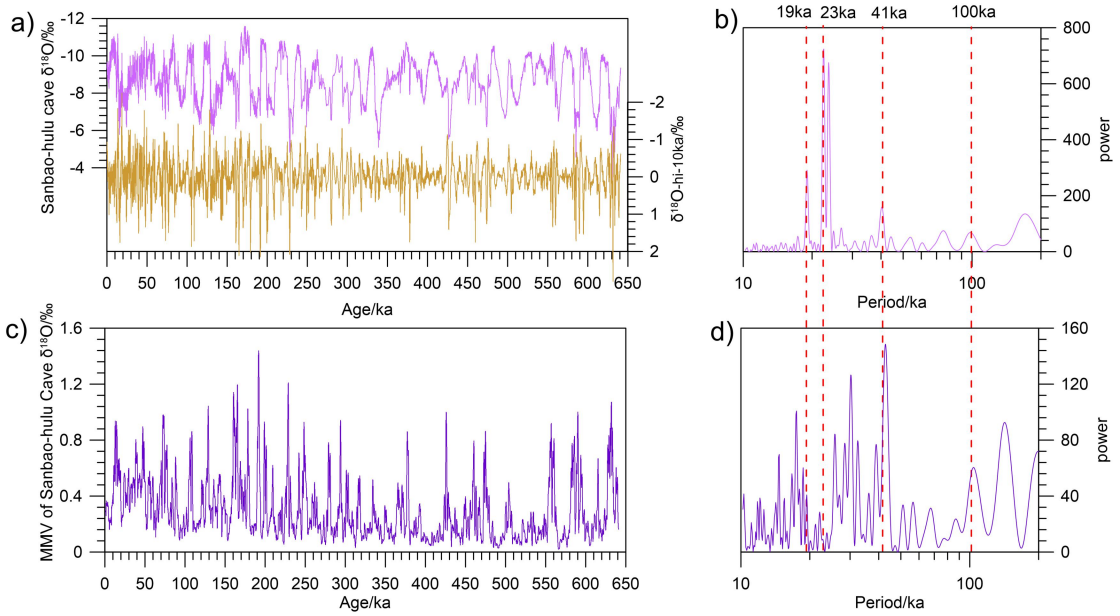


Fig. S2 Raw datasets, millennial-scale components (10ka high pass filtering signals) and MMV of the speleothem d18O record over the past 650 ka with their corresponding spectra. The orbital bands are marked with red dashed lines (eccentricity-100 ka, obliquity-41 ka ,precession-23 ka and 19 ka).

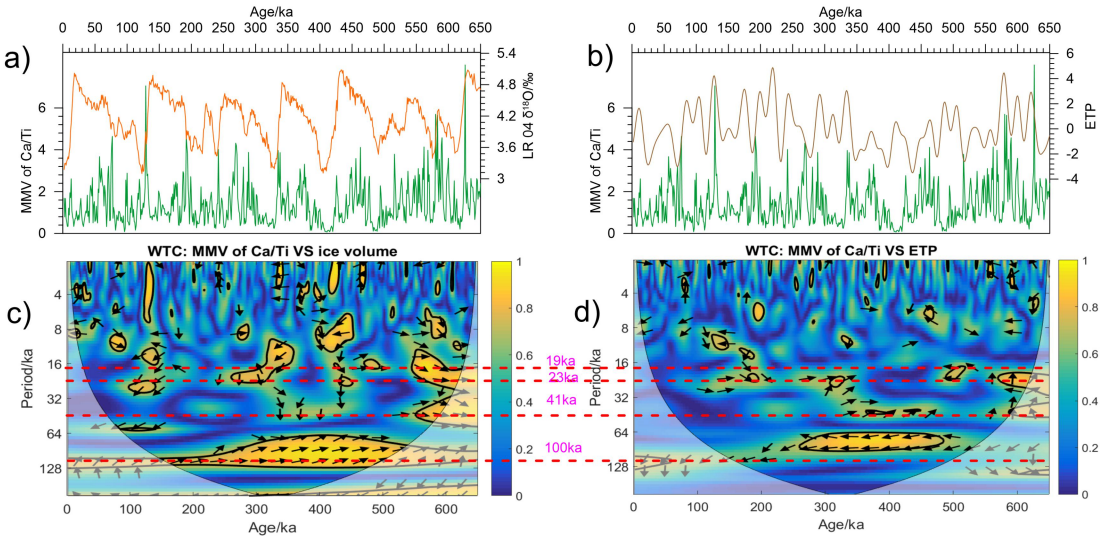


Fig. S3 Comparison of a) ice volume and b) ETP forcing for MMV of Linxia loess Ca/Ti; Wavelet coherence between c) ice volume, d) ETP and MMV of loess Ca/Ti over the past 650 ka. The orbital bands are marked with red dashed lines (eccentricity-100 kyr, obliquity-41 kyr , precession-23 kyr and 19 kyr). The black outlines denote coefficients of determination greater than 0.76. The black arrows represent the phase relationships with rightward, upward and downward arrows indicating in-phase, leading and lagging prase, respectively. Strong eccentricity, weak obliquity and precession bands ice volume modulation are observed for MMV of loess Ca/Ti.

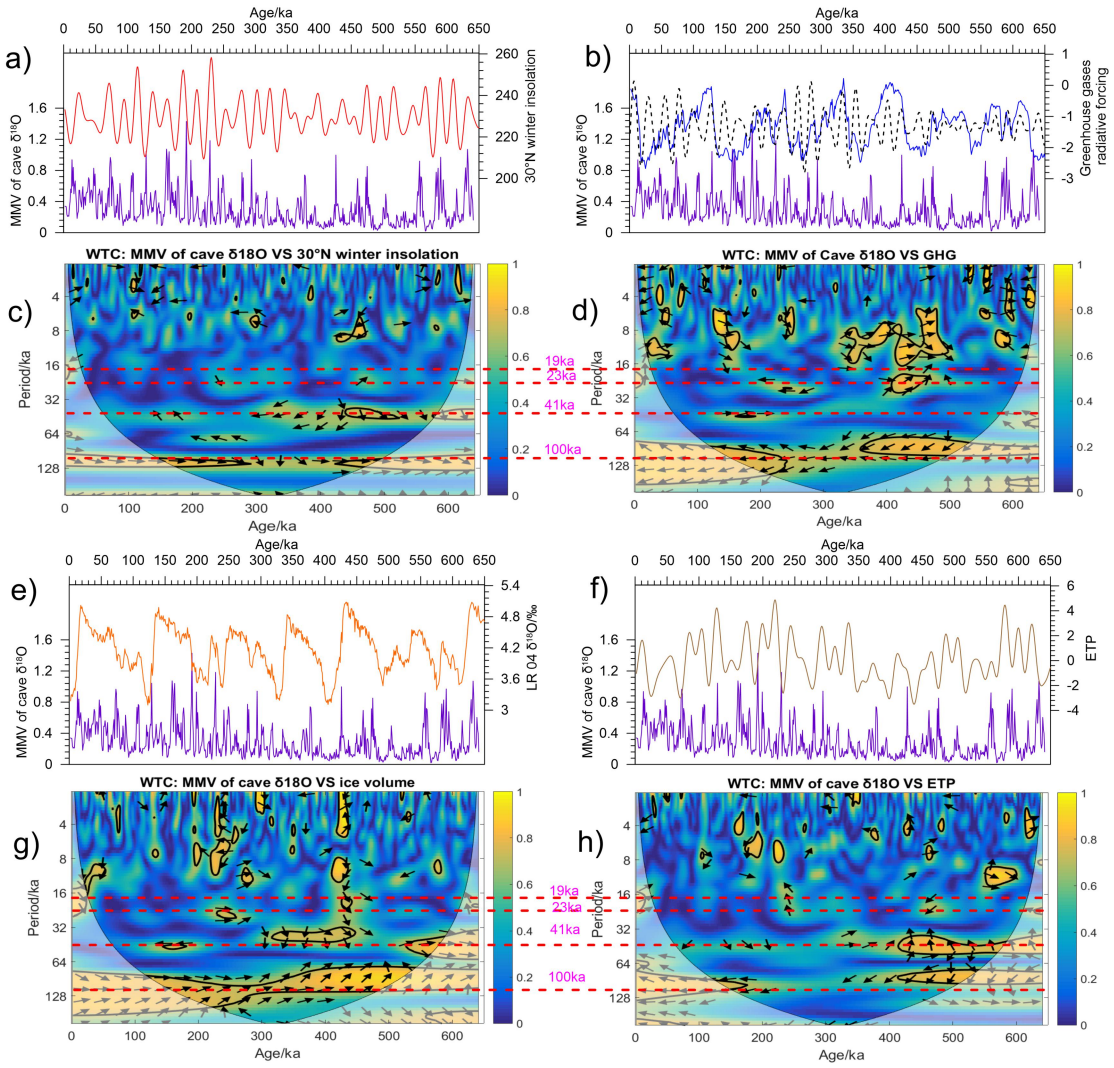


Fig. S4 Comparison of a) 30°N winter insolation, b) GHG radiative forcing (black dash line donates the precession band-pass filtering results of GHG), e) ice volume and f) ETP forcing for MMV of speleothem $\delta^{18}O$; Wavelet coherence between c) 30°N winter insolation, d) GHG, g) ice volume, h) ETP and MMV of speleothem $\delta^{18}O$ over the past 640 ka. The orbital bands are marked with red dashed lines (eccentricity-100 kyr, obliquity-41 kyr , precession-23 kyr and 19 kyr). The black outlines denote coefficients of determination greater than 0.76. The black arrows represent the phase relationship with rightward, upward and downward arrows indicating in-prase, leading and lagging phrase, respectively. Strong ice volume, GHG and winter insolation modulation at 100 kyr band, relative weak ice volume and winter insolation forcing as well as unclear precession band modulation are observed for MMV of speleothem $\delta^{18}O$.